Asian Journal of Chemistry; Vol. 35, No. 12 (2023), 3071-3080

ASIAN JOURNAL OF CHEMISTRY

https://doi.org/10.14233/ajchem.2023.30725

Geometrical Optimization and Natural Bond Orbital Analysis of Relevant Structures in the Diastereoselective Cuprate Conjugate Addition Reaction of α,β-Unsaturated Lactams using Density Functional Theory

ANAN HAJ ICHIA ARISHA[1,2,3]

[1]Department of Organic Chemistry, School of Chemistry, Faculty of Exact Sciences, Tel Aviv University, Tel Aviv 6997801, Israel
[2]Department of Education, Beit Berl College, Beit Berl, Israel
[3]Al-Qasemi Academic College, Baqa El-Gharbia 3010000, Israel

Corresponding author: E-mail: ananarisha@gmail.com

Received: 18 October 2023; *Accepted*: 8 November 2023; *Published online*: 2 December 2023; AJC-21471

In this study, density functional theory calculations at the wB97XD/Def2TZVPP level were performed to analyze the mechanism underlying the cuprate conjugate addition reaction of α,β-unsaturated lactams. The calculation results were well-aligned with those obtained experimentally–the keto-aminal and aldo-aminal, *i.e.* **2** and **1a**, yield the *syn*- and *anti*-products, respectively. The diastereoselectivity reversal originates from the small differences in the structure of the reactants. The pyramidalization and C7N3C2 angle between the aminal carbon, nitrogen and carbonyl carbon are large in **2**. The dihedral angle of the aminal oxygen, aminal carbon, nitrogen and carbonyl carbon, O8C7N3C2, is closer to 180º in **2** than in **1a**. The NBO analysis revealed string interactions between the lone pair of N3 and carbonyl π^*(O1–C2) bond. These results validate the assumption—the planarity around nitrogen in molecule **2** increases the nucleophilicity of the carbonyl oxygen, thereby driving the reaction between molecule **2** and trimethylsilyl chloride (TMSCl), which yields a siloxyiminium cation **5b** and this **5b** propels the *syn* addition of dimethylcuprate, leading to the formation of complex **7**. The π(C5–C6) (HOMO) and π^*(C2–N3) (LUMO) interactions in the siloxyiminium cation explain the increased C5–C6 double bond electrophilicity. The aldo-aminal **1a** directly reacts with dimethylcuprate under steric control and yields the *anti* complex **6a**, whose π character is stronger than that of the *syn* complex **7** and this weak π characteristics of **7** increases its stability to compensate for the trimethylsilyl disturbance. The bicyclic α,β-unsaturated lactam **8** does not contain aminal oxygen and thus remains unreactive during the cuprate conjugate addition reaction. Moreover, its pyramidalization is higher than that of the keto-aminal **2** and its dihedral angle of C8C7N3C2 is closer to 180º. Finally, a thermodynamic *anti* product is obtained, which is more stable than the *syn*-product because of less torsional strain.

Keywords: Diastereoselectivity, Conjugate addition, α,β-Unsaturated lactams, Density functional theory, Natural bond orbital.

INTRODUCTION

Conjugate addition (1,4-addition) to α,β-unsaturated carbonyls, leading to the formation of C–C bonds, is one of the most diverse reactions [1-6] and a crucial tool for organic synthesis. In addition, the Gilman reagent is one of the most outstanding reagent among its counterparts for this reaction. For example, lithium dimethylcopper $(CH_3)_2CuLi$ can be prepared by adding copper(I) iodide to methyllithium in tetrahydrofuran at –78 ºC and this nucleophilic reagent reacts with electrophiles like α,β-unsaturated carbonyl as illustrated in **Scheme-I**.

Wright *et al.* [7,8] investigated the stereochemical outcome of the conjugate addition of organocopper reagents to bicyclic α,β-unsaturated lactams derived from pyroglutaminol in the presence of trimethylsilyl chloride (TMSCl). According to their foundations, the stereochemistry of the product depends on the structure of the reactants. If the reaction is triggered with the addition of the reactant aldo-aminal **1**, then an *anti* product

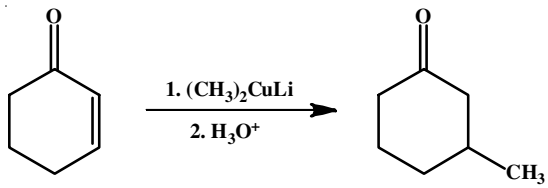

Scheme-I: 1,4-Addition of $(CH_3)_2CuLi$ to cyclohex-2-enone

This is an open access journal, and articles are distributed under the terms of the Attribution 4.0 International (CC BY 4.0) License. This license lets others distribute, remix, tweak, and build upon your work, even commercially, as long as they credit the author for the original creation. You must give appropriate credit, provide a link to the license, and indicate if changes were made.

is obtained, whereas keto-aminal **2** as a reactant yields a *syn* product as shown in **Scheme-II**.

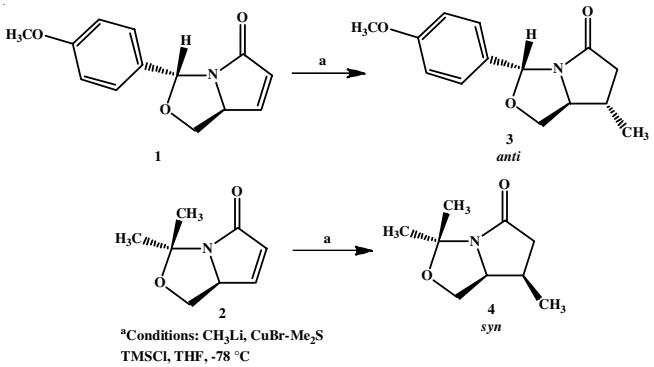

Scheme-II: Conjugate addition of $(CH_3)_2CuLi$ to a,b-unsaturated bicyclic lactams **1** and **2**

In a previous study, the *syn*-conjugate addition mechanism was adopted to synthesise inhibitors of interleukin-1 receptor associated kinase 4 (IRAK4) [9-11]. Wright *et al.* [7-9] suggested two different routes to elucidate the reversal of diastereo-selection. The *syn*-conjugate addition mechanism involves the formation of siloxyiminium ions followed by their comple-xation with copper depicted in **Scheme-III**. Since dimethyl-cuprate reacts with trimethylsilyl derivative, the **TS-1** structure is preferentially produced, which can be attributed to stereo-chemistry and leads to the formation of a *syn* product.

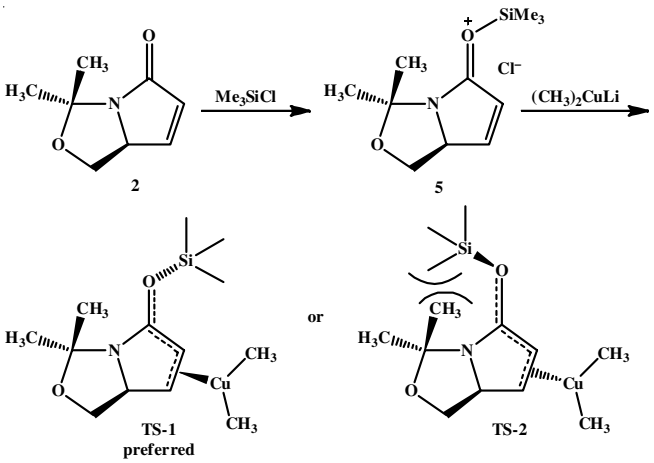

Scheme-III: *syn*-Conjugate addition

By contrast, during the anti-conjugate addition, the formation of the cuprate complex precedes the TMSCl coordination step, which then yields a sterically preferential *anti* structured product as illustrated in **Scheme-IV**. The observed differing diastereoselectivities can be attributed to the geometric structures of the reactants. X-ray-based analyses revealed that [7] the C7N3C2 angles in **1** and **2** are 122º and 127.5º, respectively, Fig. 1, which implies that the structure of **2** is more planar around nitrogen than that of **1**. Furthermore, because of the pyramidalization of the nitrogen atoms [12], the sums of the C–N–C bond angles are 343.4º and 348.9º in **1** and **2**, respectively. Notably, as the angle value approaches 360º, the planarity of the structure increases. Finally, the dihedral angle formed by the O8C7N3C2 atoms in **2** (137.3º) is larger than that in **1** (130.3º) [13].

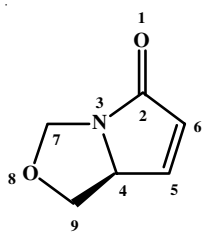

Fig. 1. Skeleton of α,β-unsaturated bicyclic lactams

Although these geometrical differences are insignificant, the diastereoselectivity essentially changes, implying that the aldo-aminal, *i.e.* **1** yields an *anti* product, whereas the keto-aminal, *i.e.*, **2**, induces the formation of a *syn* product. Wright *et al.* [7] termed this phenomenon as "small change, big impact". The small planetary changes around the nitrogen atoms significantly affects the stereoselectivity. Because of the more planar structure of **2**, structure **B** donates more to the resonance hybrid [14] as shown in Fig. 2. In addition, the oxygen atom becomes more nucleophilic and easily reacts with TMSCl to produce the siloxyiminium derivative and thus, the reaction progresses toward *syn* addition.

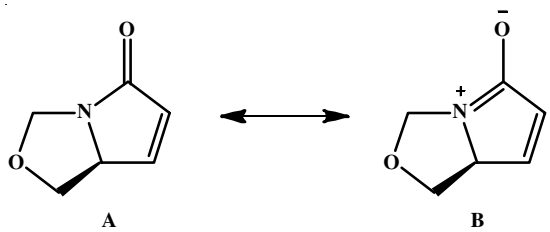

Fig. 2. Resonance structures of α,β-unsaturated bicyclic lactams

Furthermore, the reduction potentials of α,β-unsaturated carbonyl compounds play a crucial role in determine the reaction products. According to House *et al.* [15,16], 1,4-conjugate addition reaction of α,β-unsaturated carbonyl compounds

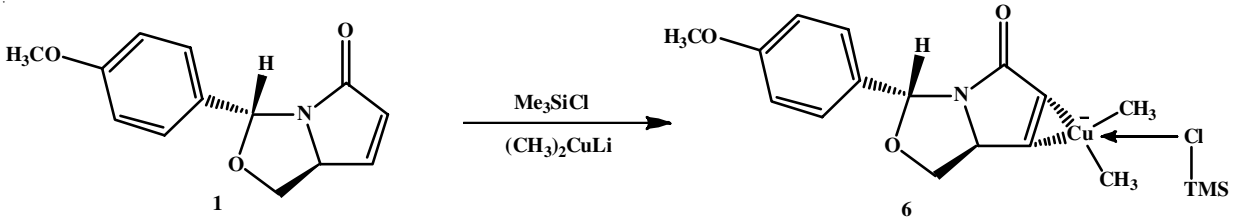

Scheme-IV: *anti*-Conjugate addition

proceeds when the reduction potential is in the range from –1.2 to –2.4 V. When the reduction potential is higher (*i.e.* less negative) than –1.2 V, saturation of the α,β-unsaturated carbonyl compound is observed, whereas no reaction with cuprate occurs when the reduction potential is lower (*i.e.*, more negative) than –2.4 V. This study was focused on the geometrical optimization and natural bond orbital (NBO) analysis of selected structures involved in the diastereoselective cuprate conjugate addition reaction of α,β-unsaturated lactams. Density functional theory (DFT) calculations were performed to gain insights into the diastereoselective mechanism that drives this addition reaction.

COMPUTATIONAL METHODS

Density functional theory (DFT) calculations were performed using the Gaussian 16 software [17] and GaussView 6.0 interface [18]. All the geometric optimizations and frequency calculations were performed using the wB97XD-DFT method, which included empirical dispersion and long-range corrections. The valence and triple zeta Def2TZVPP was utilized as the basis set and all the stationary points were identified as minima (zero imaginary frequencies). The NBO calculations were performed at the same level of theory. The values of the total energy with thermal correction (ΔE), enthalpy (ΔH) and Gibbs energy (ΔG) were obtained under the standard conditions of 298.15 K and 1 atm in gas phase.

RESULTS AND DISCUSSION

Diastereoselectivity strongly depends on the structure of the reactants and thus, the structures of **1a** (aldo-aminal) and **2** (keto-aminal) were optimized and the resulting structures are shown in Fig. 3. Some of the associated geometric parameters are listed in Table-1. The N3–C2 length in **2** is slightly shorter than that in **1a**, while that of C2–O1 in the former is slightly longer than that in the latter structure.

The C7N3C2 angle, pyramidalization and dihedral angle of O8C7N3C2 in **2** are consistent with those obtained *via* experiments [7] as well as higher than those in **1a**, as evidenced

TABLE-1
SOME SELECTED GEOMETRIC PARAMETERS OF **1a** AND **2**

	Compound **1a**	Compound **2**
Selected bond lengths (Å)		
N3–C2	1.3838	1.3803
C2–O1	1.2074	1.2089
C7–N3	1.4608	1.4710
O8–C7	1.4196	1.4322
O8–C9	1.4116	1.4105
C5–C6	1.3283	1.3277
C6–C2	1.4898	1.4913
Selected bond angles (°)		
C7N3C2	121.8942	127.5005
C7N3C4	110.0705	110.2210
C4N3C2	110.7588	111.2607
Sum of CNC angles (pyramidalization)	342.7235°	348.9822°
Dihedral angle of O8C7N3C2	-131.1902°	-137.3001°

from Table-1. These calculated results indicate that the planarity around nitrogen is higher in **2** than in **1a** and validate the assumption (reported in previous studies) that the diastereoselectivity conjugate addition of cuprate to α,β-unsaturated lactams depends on the planarity of nitrogen. Although the difference in C7N3C2 is only 5.6063° and that in the pyramidalization is 6.2587°, these small changes reverse the addition type from *syn* for **2** to *anti* for **1**. Because of the high planarity around the nitrogen in **2**, the nitrogen lone pair (LP) of electrons is donated to the carbonyl bond and this phenomenon increases the contribution of structure **B** to the resonance hybrid as shown in Fig. 2.

To examine the validity of this assumption, NBO analysis was conducted in the present study. NBO analysis is a robust tool for evaluating the interactions between the donor and acceptor orbitals of a molecule and provides significant insights into such bonding interactions. The stabilization energy E(2) associated with the electron delocalization between Lewis (filled) and non-Lewis (unfilled) NBOs is estimated as:

$$E(2) = \Delta E_{i,j} = -q_i \frac{F^2(i,j)}{\varepsilon_i - \varepsilon_j}$$

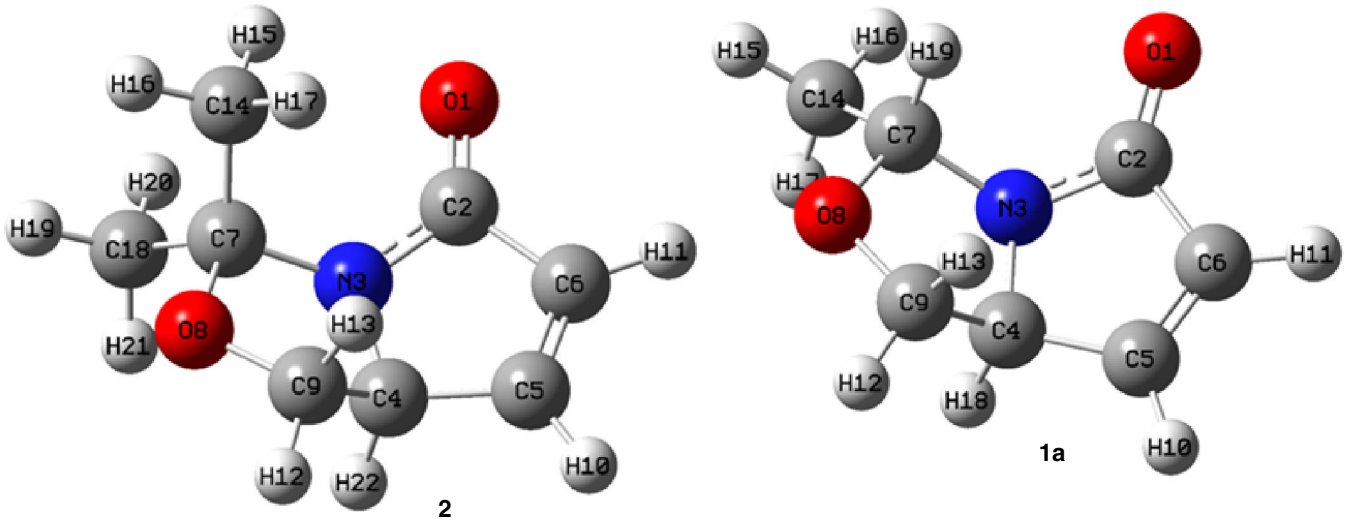

Fig. 3. Optimized structures of **1a** and **2**

where q_i is the donor orbital occupancy, ε_i and ε_j are diagonal elements and F(i,j) is the Fock matrix element. The strength of the interactions between electron donors and acceptors is proportional to the stabilization energy E(2). The relevant NBO analysis results of **1a** and **2** are presented in Tables 2 and 3, respectively.

TABLE-2
ANALYSIS OF THE FOCK MATRIX IN THE NBO BASIS FOR **1a** USING SECOND-ORDER PERTURBATION THEORY

Donor NBO (i)	Acceptor NBO (j)	E(2) (kcal/mol)	E(i)-E(i) (a.u.)	F(i,i) (a.u.)
π(C5–C6)	π*(O1–C2)	24.04	0.44	0.097
LP (O1)	σ*(C2–N3)	36.77	0.81	0.157
LP (O1)	σ*(C2–C6)	28.96	0.78	0.137
LP (N3)	π*(O1–C2)	64.74	0.43	0.150
LP (O8)	σ*(N3–C7)	3.52	0.78	0.047
π*(O1–C2)	π*(C5–C6)	52.85	0.02	0.073

TABLE-3
ANALYSIS OF THE FOCK MATRIX IN THE NBO BASIS FOR **2** USING SECOND-ORDER PERTURBATION THEORY

Donor NBO (i)	Acceptor NBO (j)	E(2) (kcal/mol)	E(i)-E(i) (a.u.)	F(i,i) (a.u.)
π(C5–C6)	π*(O1–C2)	23.61	0.44	0.096
LP (O1)	σ*(C2–N3)	36.91	0.82	0.157
LP (O1)	σ*(C2–C6)	28.53	0.78	0.136
LP (N3)	π*(O1–C2)	73.51	0.41	0.156
LP (O8)	σ*(N3–C7)	4.28	1.06	0.060
π* (O1–C2)	π* (C5–C6)	51.84	0.02	0.073

Tables 2 and 3 indicate that the strength of the interaction between the LP of N3 and π*(O1–C2) is the highest and the corresponding E(2) is 73.51 kcal/mol for **2** and 64.74 kcal/mol for **1a**. In both compounds **1a** and **2**, the donor orbital is HOMO-1 concentrate on N3, while the acceptor orbital is the LUMO carbonyl anti-bonding π.

The corresponding orbitals of **1a** are illustrated in Fig. 4 and the same pattern is observed in the case of **2**. No significant interactions are detected between the N3 LP and σ*(O1–C2). Because of this interaction between the nitrogen LP and carbonyl group, the oxygen atom becomes sufficiently nucleophilic to react reversibly with TMSCl and yields the siloxyiminium ion.

Aldo-aminal **1a** reacts only with active TMSBr or TMSI, although in the presence of TMSCl, it reacts first with the cuprate [7]. The optimized structures of the siloxyiminium cations **5a** and **5b** are depicted in Fig. 5 and Table-4 presents some of their selected geometric parameters.

TABLE-4
SOME SELECTED GEOMETRIC PARAMETERS OF **5a** AND **5b**

	5a	**5b**
Selected bond lengths (Å)		
N3–C2	1.3180	1.3160
C2–O1	1.2724	1.2741
C7–N3	1.4812	1.4942
O8–C7	1.4057	1.4190
O8–C9	1.4137	1.4123
C5–C6	1.3376	1.3369
C6–C2	1.4607	1.4621
O1–Si	1.7612	1.7556
Selected bond angles (°)		
C7N3C2	128.8347	132.3148
C7N3C4	110.7001	110.7270
C4N3C2	110.7312	110.7199
C2O1Si	132.2487	132.5785
Sum of CNC angles (pyramidalization)	350.2660°	353.7617°
Dihedral angle (°)		
O8C7N3C2	-140.2599	-145.7773
N3C2O1Si	179.9614	176.0670

In both **5a** and **5b**, the nitrogen and silicon atoms are *anti* planar and are thus more stable than the *syn* conformation, while trimethylsilyl is located far from C7. The C7N3C2 angle, pyramidalization and dihedral angle of O8C7N3C2 in **5b** are

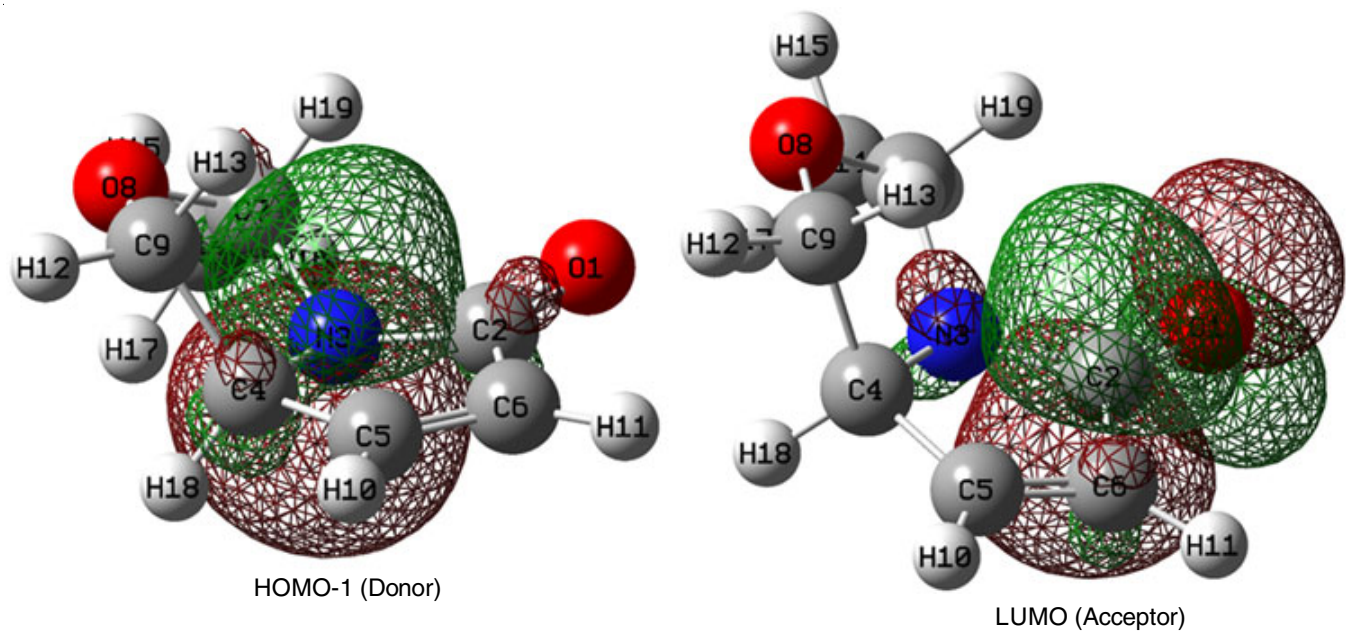

Fig. 4. HOMO-1 and LUMO of **1a**

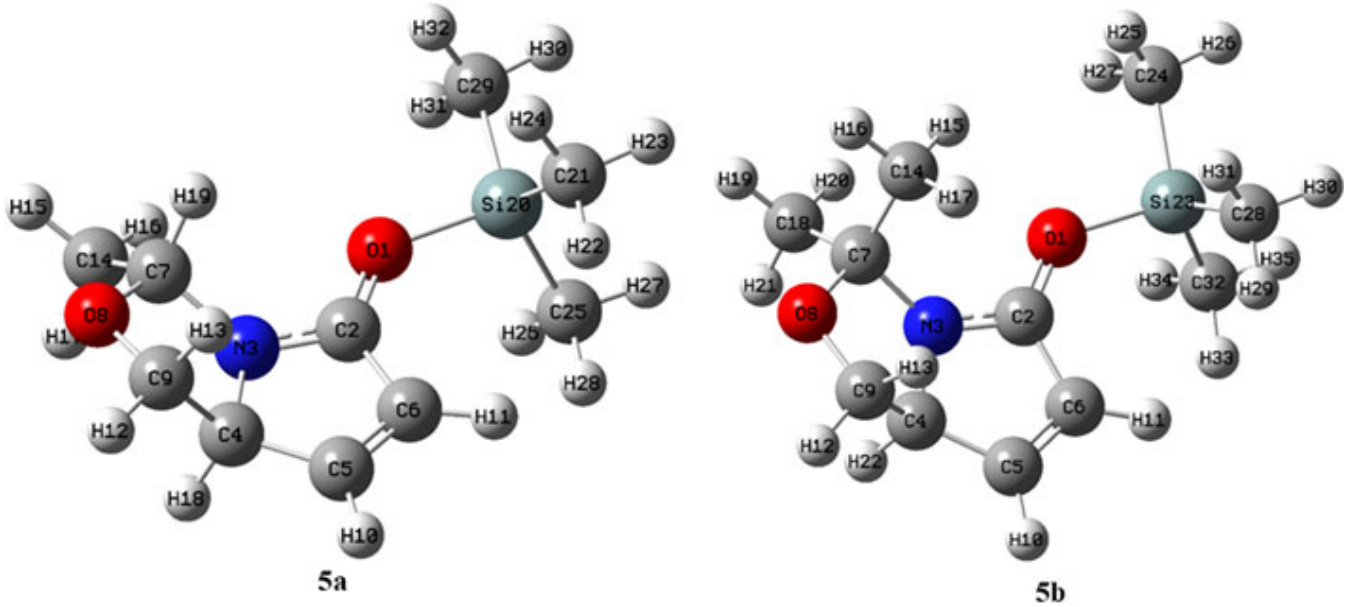

Fig. 5. Optimized structures of the siloxyiminium cations **5a**, **5b**

larger than those in **5a**, suggesting that the planarity around nitrogen is retained in the siloxyiminium cations as well. Further, preferred formation of **5a** can be partially ascribed to its O1–Si bond, which is slightly shorter than that in **5a**, as evidenced from Table-4. Therefore, a detailed NBO analysis was conducted to evaluate the orbital interactions in **5a** and **5b** and the corresponding results are shown in Tables 5 and 6.

TABLE-5
ANALYSIS OF THE FOCK MATRIX IN THE NBO BASIS FOR **5a** USING SECOND-ORDER PERTURBATION THEORY

Donor NBO (i)	Acceptor NBO (j)	E(2) (kcal/mol)	E(i)-E(i) (a.u.)	F(i,j) (a.u.)
π(C5–C6)	π*(C2–N3)	38.25	0.36	0.112
σ(O1–Si20)	σ*(C2–N3)	8.39	1.41	0.098
LP (O1)	σ*(C2–C6)	16.32	1.06	0.118
LP (O1)	π*(C2–N3)	99.23	0.40	0.185
π*(C2–N3)	π*(C5–C6)	15.84	0.09	0.070
LP (O8)	σ*(N3–C7)	3.29	1.02	0.052
σ(C2–N3)	σ*(O1–Si20)	3.07	1.28	0.057
σ(C4–N3)	σ*(O1–C2)	7.28	1.36	0.089
σ (C5–C6)	σ*(O1–C2)	5.61	1.39	0.079

TABLE-6
ANALYSIS OF THE FOCK MATRIX IN THE NBO BASIS FOR **5b** USING SECOND-ORDER PERTURBATION THEORY

Donor NBO (i)	Acceptor NBO (j)	E(2) (kcal/mol)	E(i)-E(i) (a.u.)	F(i,j) (a.u.)
π(C5–C6)	π*(C2–N3)	37.54	0.37	0.112
σ(O1-Si23)	σ*(C2–N3)	8.67	1.42	0.100
LP (O1)	σ*(C2–C6)	15.97	1.06	0.117
LP (O1)	π*(C2–N3)	97.09	0.41	0.184
π*(C2–N3)	π*(C5–C6)	16.24	0.09	0.071
LP (O8)	σ*(N3–C7)	4.37	1.00	0.060
σ(C2–N3)	σ*(O1–Si23)	3.17	1.28	0.058
σ(C4–N3)	σ*(O1–C2)	7.57	1.36	0.091
σ(C5–C6)	σ*(O1–C2)	5.49	1.39	0.078

Two essential donor–acceptor interactions are observed in the **5a** and **5b** structures. First, the interaction between the donor LP of O1 (HOMO-2) and LUMO acceptor π*(C2–N3) can be ascribed to the negative O1, which is bonded to electro positive Si. Second, the critical interaction between π(C5–C6) (HOMO) and π*(C2–N3) LUMO (Tables 5 and 6) increases the π(C5–C6) electrophilicity in the siloxyiminium cation during the cuprate addition. The HOMO and LUMO of **5b** are shown in Fig. 6.

Another hypothesis [7] for the diastereoselective cuprate conjugate addition reaction is the development of a positive charge on O8, which may attract the nucleophilic cuprate reagent. The recalculated NBO charges of some atoms in **2**, **5b**, **1a** and **5a** are shown in Table-7. As the reaction proceeds from bicyclic α,β-unsaturated lactams to siloxyiminium cations, the charge changes only negligibly, indicating that the effect of the charge on O8 on the cuprate addition mechanism is insignificant.

Moreover, Tables 5 and 6, indicate that the donor LP O8 weakly interacts with the acceptor σ*(N3–C7) and may introduce some positive charges on O8. The siloxyiminium cation **5b** undergoes *syn* reaction with dimethylcuprate and yields complex **7**, whose optimized structure and some selected geometric parameters are presented in Fig. 7 and Table-8, respectively. During the addition of nucleophilic dimethylcuprate to **5b**, the C2–C6 and O1–Si23 bonds shorten, whereas the length of the C2–O1 and C5–C6 bonds increase because the negative dimethylcuprate moves the electron toward carbonyl. Correspondingly, the trimethylsilyl group drifts away from the copper space and finally, the Cu36–C5 bond becomes shorter than the Cu36–C6 bond because of the lateral bonding between C41, C5. Evidently, when the two methyl groups on copper are replaced with *tert*-butyl, the copper complex collapses because of steric hindrance. The internal interactions in complex **7** were investigated *via* NBO analyses and the corresponding results are shown in Table-9.

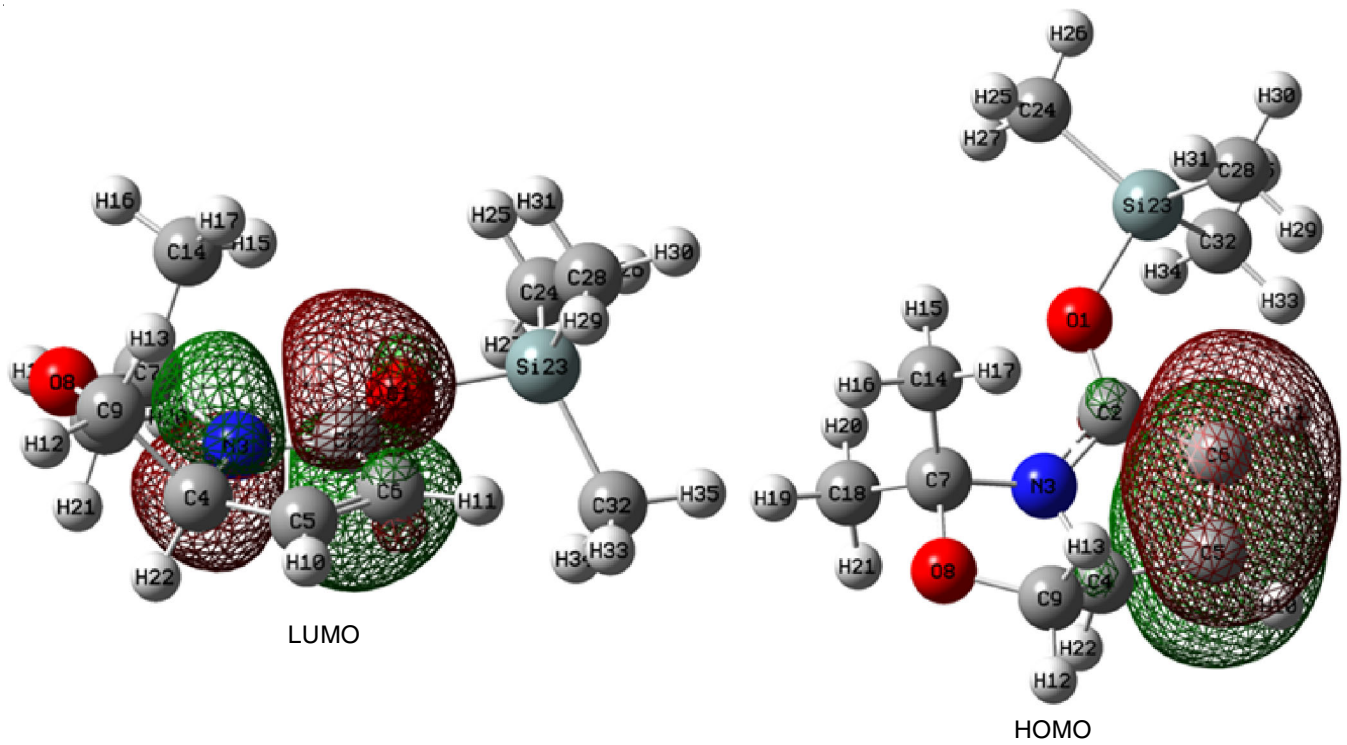

Fig. 6. HOMO and LUMO for **5a**

TABLE-7
NBO CHARGES OF SOME ATOMS IN **2**, **5b**, **1a** AND **5a**

Species	O8	C7	N3	C2	O1	C6	C5
2	-0.506	0.421	-0.437	0.632	-0.590	-0.277	-0.144
5b	-0.481	0.427	-0.334	0.669	-0.716	-0.306	-0.062
Δ(charge) charge(**5b**)-charge(**2**)	0.025	0.006	0.103	0.037	-0.126	-0.029	0.082
1a	-0.493	0.248	-0.428	0.630	-0.582	-0.281	-0.141
5a	-0.464	0.254	-0.326	0.669	-0.713	-0.308	-0.057
Δ(charge) charge(**5a**)-charge(**1a**)	0.029	0.006	0.102	0.039	-0.131	-0.027	0.084

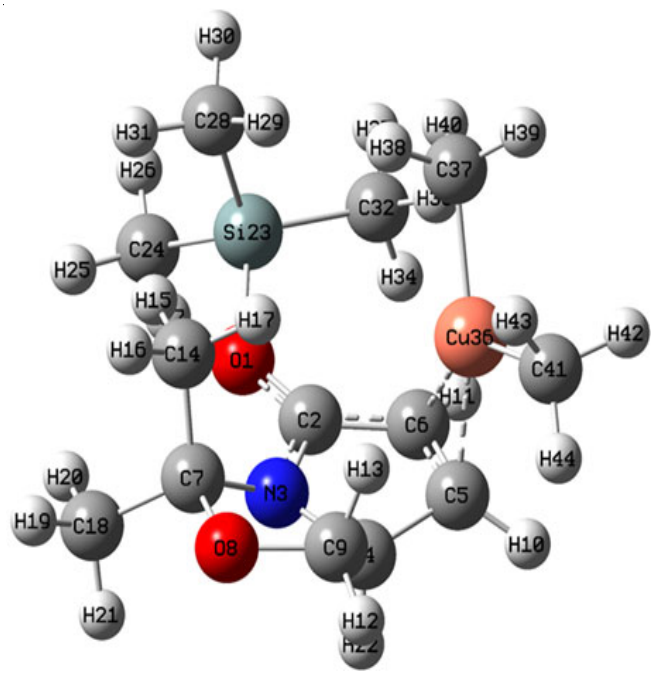

Fig. 7. Optimized structure of complex **7**

TABLE-8
SOME SELECTED GEOMETRIC PARAMETERS FOR COMPLEX **7**

Selected bond lengths (Å)		Selected bond angles (°)	
N3–C2	1.3415	C7N3C2	128.8337
C2-O1	1.3041	C7N3C4	111.0543
C7–N3	1.4784	C4N3C2	110.2149
O8-C7	1.4156	C2O1Si23	133.3319
O8-C9	1.4199	C6Cu36C41	138.2537
C5–C6	1.4520	C6Cu36C37	119.7792
C6-C2	1.4026	C5Cu36C41	96.5145
O1-Si23	1.7053	C5Cu36C37	161.7063
Cu36–C5	1.9422	C37Cu36C41	101.6978
Cu36–C6	2.0680	Dihedral angle (°)	
Cu36–C41	1.9591	O8C7N3C2	-151.0450
Cu36–C37	1.9750	N3C2O1Si23	154.9919
Sum of CNC angles (pyramidalization)			350.1029°

The σ(C5–Cu36) bond is distributed around the neighbouring bonds and C6 and consequently, C5 becomes highly electrophilic for the C41 nucleophilic attack at the *syn*-face. The negative charge is concentrated on C6 and the σ(C41–Cu36) bond, *i.e.* HOMO-7, donates electrons to the acceptor σ^*(C5–Cu36), *i.e.* LUMO+1, leading to the formation of the

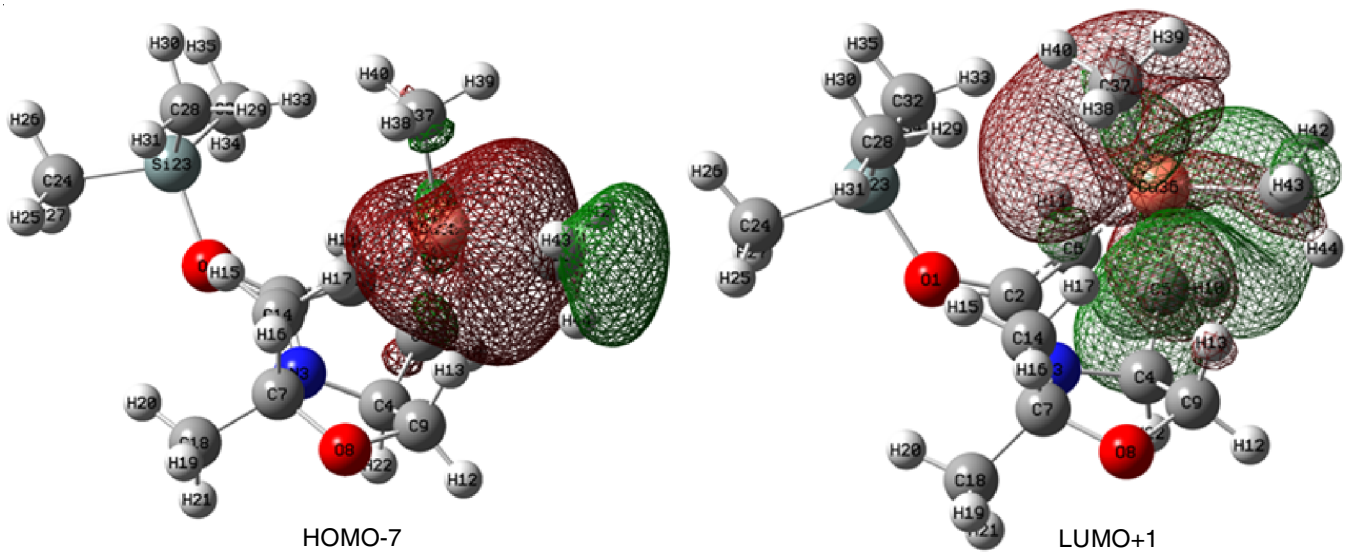

Fig. 8. HOMO-7 and LUMO+1 of complex **7**

TABLE-9
ANALYSIS OF THE FOCK MATRIX IN THE NBO BASIS FOR 7 USING SECOND-ORDER PERTURBATION THEORY

Donor NBO (i)	Acceptor NBO (j)	E(2) (kcal/mol)	E(j)-E(i) (a.u.)	F(i,j) (a.u.)
σ(C2–C6)	LP*(5) (Cu36)	13.99	1.13	0.116
σ(C4–N3)	σ*(O1–C2)	7.42	1.29	0.087
σ(C4-C5)	LP*(5) (Cu36)	7.09	1.04	0.079
σ(C5–C6)	LP*(5) (Cu36)	27.68	1.07	0.158
σ(C5–C6)	σ*(O1–C2)	9.57	1.22	0.097
σ(C5–Cu36)	LP (C6)	69.45	0.12	0.109
σ(C5–Cu36)	σ*(C5–Cu36)	17.72	0.50	0.084
σ(C5–Cu36)	σ*(C37–Cu36)	65.65	0.61	0.185
σ(C5–Cu36)	σ*(C41–Cu36)	46.50	0.53	0.141
σ(C41–Cu36)	σ*(C5–Cu36)	35.93	0.61	0.141
LP (O1)	σ*(C2–C6)	13.53	1.11	0.111
LP (O1)	π*(C2–N3)	59.05	0.44	0.158
LP (C6)	LP*(5)(Cu36)	34.75	0.51	0.143
LP (C6)	π*(C2–N3)	186.09	0.17	0.167
LP (C6)	σ*(C5–Cu36)	52.13	0.37	0.138
LP (C6)	σ*(C41–Cu36)	13.29	0.40	0.074
LP (O8)	σ*(N3–C7)	5.37	0.74	0.056
σ*(C5–Cu36)	LP*(5) (Cu36)	18.65	0.14	0.086
σ*(C5–Cu36)	σ*(C37–Cu36)	67.16	0.11	0.137
σ*(C5–Cu36)	σ*(C41–Cu36)	636.52	0.03	0.204
σ*(C37–Cu36)	LP*(5) (Cu36)	28.26	0.03	0.059
σ*(C41–Cu36)	LP*(5) (Cu36)	26.20	0.11	0.097
σ*(C41–Cu36)	σ*(C37–Cu36)	40.61	0.08	0.098

LP = Lone pair of electrons

syn product **4**. The HOMO-7 and LUMO+1 of complex **7** are depicted in Fig. 8.

The aldo-aminal (**1a**) directly reacts with dimethylcuprate in the presence of TMSCl and yields the anti-structure anion complex **6a**, whose optimized geometry and some structural parameters are shown in Fig. 9 and Table-10, respectively. The C9 and Cu20 are *anti*, which contribute to the stability of the complex. The C5–C6 exhibits double-bond characteristics and the geometry around nitrogen is less planner than that in the *syn* complex **7**. The two methyl groups around copper are far

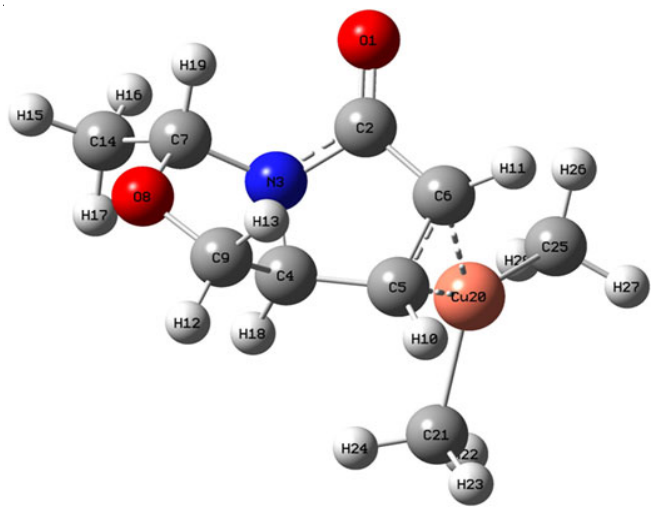

Fig. 9. Optimized structure of the anion **6a**

TABLE-10
SOME SELECTED GEOMETRIC PARAMETERS OF THE ANION **6a** (anion)

Selected bond lengths (Å)		Selected bond angles (°)	
N3–C2	1.4106	C7N3C2	119.6798
C2–O1	1.2168	C7N3C4	109.0561
C7–N3	1.4425	C4N3C2	109.7542
O8–C7	1.4333	C6Cu20C21	139.7278
O8–C9	1.4169	C6Cu20C25	112.6160
C5–C6	1.4246	C5Cu20C21	97.9486
C6–C2	1.4603	C5Cu20C25	154.3843
Cu20–C5	1.9546	C25Cu20C21	107.6384
Cu20–C6	2.0350		
Cu20–C21	1.9945	Dihedral angle (°)	
Cu20–C25	1.9938	O8C7N3C2	-115.2240
Sum of CNC angles (pyramidalization)			338.4901°

in **6a**, because in the absence of trimethylsilyl group, the complex is less crowded and thus, the structure is more relaxed.

The π-complex pattern of **6a** is revealed by the NBO analysis as shown in Table-11. Although electrons are transferred

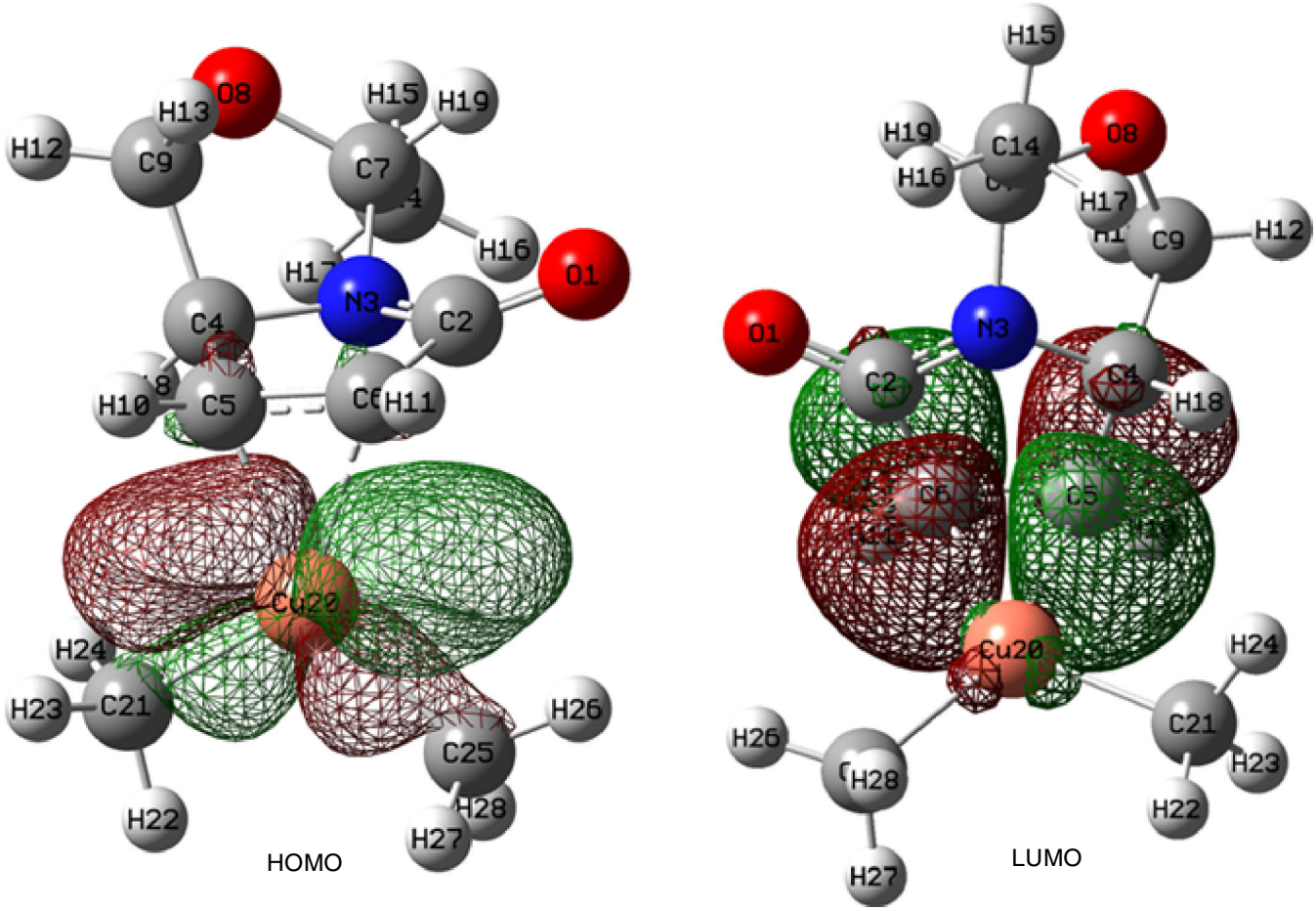

Fig. 10. HOMO and LUMO of complex **6a**

TABLE-11
ANALYSIS OF THE FOCK MATRIX IN THE NBO BASIS FOR **6a** USING SECOND-ORDER PERTURBATION THEORY

Donor NBO (i)	Acceptor NBO (j)	E(2) (kcal/mol)	E(i)-E(i) (a.u.)	F(i,i) (a.u.)
π(C5–C6)	π*(O1–C2)	25.78	0.46	0.099
LP (O1)	σ*(C2–N3)	37.48	0.78	0.155
LP (O1)	σ* (C2–C6)	24.20	0.82	0.128
LP (N3)	π*(O1–C2)	51.38	0.44	0.137
π*(C5–C6)	π*(O1–C2)	86.55	0.05	0.086
σ(C2–C6)	LP*(6) (Cu20)	11.39	1.06	0.101
σ(C4-C5)	LP*(6) (Cu20)	10.57	1.04	0.096
σ(C5–C6)	LP*(6) (Cu20)	29.97	1.07	0.164
π(C5–C6)	LP*(6) (Cu20)	62.75	0.71	0.192
σ(C21–Cu20)	π*(C5–C6)	17.87	0.41	0.087
LP (5) (Cu20)	π*(C5–C6)	113.38	0.27	0.165
LP (5) (Cu20)	σ*(C21–Cu20)	17.00	0.65	0.105
LP (5) (Cu20)	σ*(C25–Cu20)	10.67	0.62	0.081
LP* (6) (Cu20)	σ*(C25–Cu20)	11.70	0.05	0.071

LP = Lone pair of electron

(donated) from C5–C6 to copper, a strong back donation ability from Cu (HOMO) to the LUMO, π* (C5–C6), is observed; this interaction is represented in Fig. 10. The orientation of C21 is suitable for its reaction with C5 and an *anti* product is derived in this process.

The presence of O8 in the α,β-unsaturated lactams is crucial for the conjugate addition reaction. In compound **8**, O8 is replaced by a methylene group as shown in Fig. 11. The geometric data and NBO analysis results of **8** are provided in Tables 12 and 13, respectively. Interestingly, the pyramidalization in **8** is higher than that in **2** and the dihedral angle of C8C7N3C2 is closer to 180º. These results demonstrate that **8** is more planar around nitrogen, leading to strong interactions the nitrogen LP and π*(O1–C2), as shown in Table-13. Although these strong interactions drive the reaction with TMSCl, the C5–C6 double bond electrophilicity is not sufficient for the reaction with the dimethylcuprate reagent.

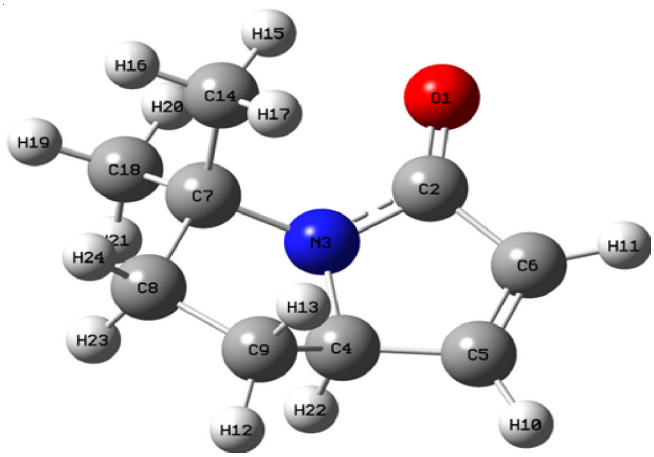

Fig. 11. Optimized structure of **8**

TABLE-12
SOME SELECTED GEOMETRIC PARAMETERS OF **8**

Selected bond lengths (Å)	
N3–C2	1.3727
C2-O1	1.2121
C7–N3	1.4750
C8-C7	1.5491
C8-C9	1.5310
C5–C6	1.3282
C6-C2	1.4924
Selected bond angles (°)	
C7N3C2	127.1186
C7N3C4	113.0001
C4N3C2	111.6191
Sum of CNC angles (pyramidalization)	351.7378°
Dihedral angle of C8C7N3C2	-147.3013°

TABLE-13
ANALYSIS OF THE FOCK MATRIX IN THE NBO BASIS FOR **8** USING SECOND-ORDER PERTURBATION THEORY

Donor NBO (i)	Acceptor NBO (j)	E(2) (kcal/mol)	E(i)-E(i) (a.u.)	F(i,j) (a.u.)
π(C5–C6)	π*(O1–C2)	23.18	0.44	0.096
LP (O1)	σ*(C2–N3)	35.27	0.83	0.155
LP (O1)	σ*(C2–C6)	28.52	0.78	0.135
LP (N3)	π*(O1–C2)	80.20	0.40	0.160
π*(O1–C2)	π*(C5–C6)	51.91	0.02	0.074

Finally, the thermodynamic effect is evaluated. The assumed structures of the *syn*- and *anti*-products, which may form during the reaction of **2** or **1a** with dimethylcuprate, are optimized and their thermodynamic parameters are calculated (Table-14). The *anti* product is more stable because of less torsional strain with C9. *anti* **3a** is more stable than *anti* **4a** and therefore, in the aldo-animal (**1a**), the *anti* face leads to the formation of a thermodynamic product because of steric control. However, in **2**, because of the formation of siloxyiminium cation, the *syn* face is preferred for the cuprate addition, although this reaction yields a less stable product, *viz. syn* **4** (Fig. 12). In the presence of TMSCl, the formation of a siloxyiminium cation is observed in **2** but not in **1a**. Therefore, the trimethylsilyl transfer ability of **5a** is expected to be stronger than that of **5b** as confirmed by the calculations (Table-14, eqn. 3).

TABLE-14
STANDARD GIBBS ENERGY CHANGE FOR SOME SELECTED REACTIONS

Reaction	ΔG° (kcal/mol)
4 (syn) → **4a** (anti)	-1.29
3b (syn) → **3a** (anti)	-1.95
5a + **2** → **5b** + **1a**	-2.16

Conclusion

In this study, the cuprate conjugate addition reaction of α,β-unsaturated lactams was analyzed by DFT calculations at the wB97XD/Def2TZVPP level. The calculation results are in good agreement with the previously reported experimental ones, which demonstrated the reversal of diastereoselection from *anti* to *syn* while the reaction proceeds from aldo-aminal **1a** to keto-aminal **2**. Compared to **1a**, **2** exhibits large C7N3C2 angle and pyramidalization, in addition to a ~ 180º dihedral angle O8C7N3C2. The NBO analysis revealed strong interactions between the LP of N3 and π*(O1–C2) bond. These foundations reinforce the assumption that the high planarity around nitrogen in **2** increases the nucleophilicity of the carbonyl oxygen, enabling the reaction between **2** and TMSCl, which yields siloxyiminium cations. In siloxyiminium cation, the nitrogen and silicon atoms are *anti* planar and this structure drives dimethylcuprate to attack the *syn*-face. Further, the increased C5–C6 double bond electrophilicity can be attributed to the π(C5–C6) (HOMO) and π*(C2–N3) LUMO interactions in the siloxyiminium cation. The increased positive charge on O8 in the siloxyiminium cation may be attract the nucleophilic cuprate reagent, but its effect is negligible. The aldo-aminal (**1a**) directly reacts with dimethylcuprate under steric control to yield the *anti* complex **6a**, which exhibits superior π characteristics compared to the *syn* complex **7** complex. This phenomenon endows additional stability to **7** to compensate for the

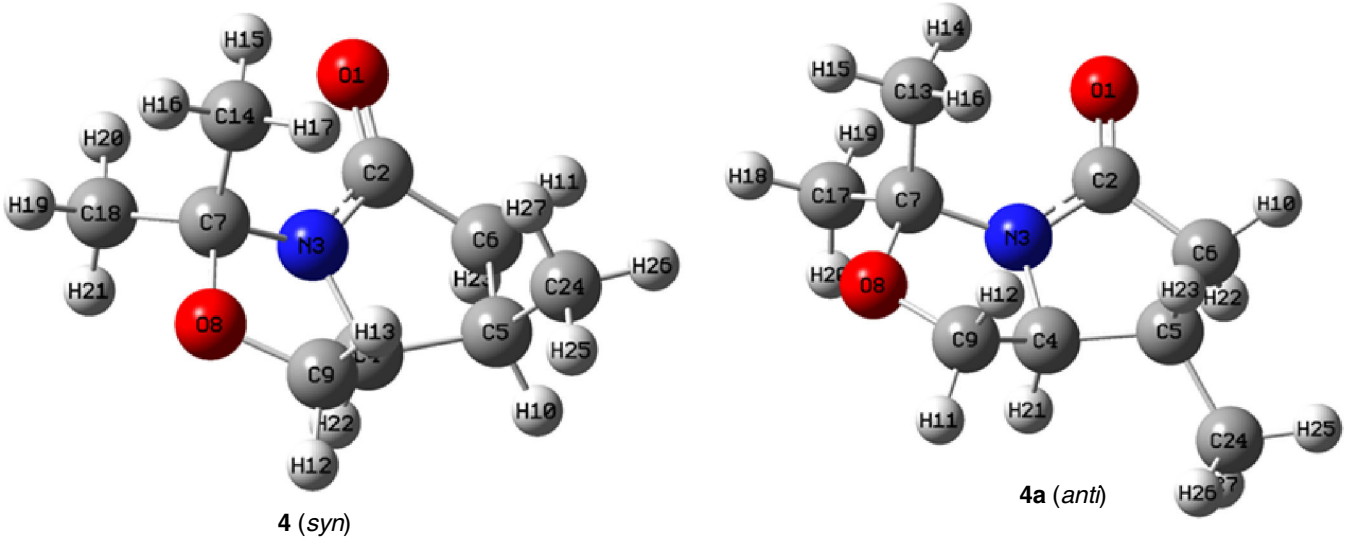

4 (*syn*) **4a** (*anti*)

Fig. 12. Optimized structures of **4** and **4a**

trimethylsilyl disturbance. The bicyclic α,β-unsaturated lactam (**8**), which lacks aminal oxygen, is unreactive in the cuprate conjugate addition reaction. Its pyramidalization is higher than that of the keto-aminal (**2**) and the dihedral angle of C8C7N3C2 is closer to 180. Furthmore, **8** is more planar around nitrogen and activates the reaction with TMSCl; however, the C5–C6 double bond electrophilicity is not sufficient for the reaction with dimethylcuprate. Thus, a balance between the nucleophilicity of the carbonyl oxygen and electrophilicity of C=C is essential. The final *anti* product exhibits thermodynamical characteristics and is more stable than the *syn* product because of less torsional strain. Finally, the trimethylsilyl transfer ability of **5a** is stronger than that of **5b**. The findings of this study are anticipated to propel more such investigations on method to isolate crucial copper complexes and gain more insights in to underlying mechanism of this interesting reaction.

CONFLICT OF INTEREST

The authors declare that there is no conflict of interests regarding the publication of this article.

REFERENCES

1. E.J. Corey and N.W. Boaz, *Tetrahedron Lett.*, **26**, 6019 (1985); https://doi.org/10.1016/S0040-4039(00)95114-1
2. E.J. Corey and N.W. Boaz, *Tetrahedron Lett.*, **26**, 6015 (1985); https://doi.org/10.1016/S0040-4039(00)95113-X
3. Y. Horiguchi, S. Matsuzawa, E. Nakamura and I. Kuwajima, *Tetrahedron Lett.*, **27**, 4025 (1986); https://doi.org/10.1016/S0040-4039(00)84901-1
4. S.H. Bertz and R.A.J. Smith, *Tetrahedron*, **46**, 4091 (1990); https://doi.org/10.1016/S0040-4020(01)90543-5
5. B.H. Lipshutz, S.H. Dimock and B. James, *J. Am. Chem. Soc.*, **115**, 9283 (1993); https://doi.org/10.1021/ja00073a052
6. S.H. Bertz, G. Miao, B.E. Rossiter and J.P. Snyder, *J. Am. Chem. Soc.*, **117**, 11023 (1995); https://doi.org/10.1021/ja00149a032
7. S.W. Wright, C. Choi, Y. Kawamata and P.S. Baran, *J. Org. Chem.*, **88**, 4387 (2023); https://doi.org/10.1021/acs.joc.2c02993
8. S.W. Wright, C. Choi, S. Chung, B.P. Boscoe, S.E. Drozda, J.J. Mousseau and J.D. Trzupek, *Org. Lett.*, **17**, 5204 (2015); https://doi.org/10.1021/acs.orglett.5b02533
9. S.W. Wright, B. Li, Z. Peng, L. Wei, E. McInturff, D. Place, D.B. Damon and R.A. Singer, *Org. Process Res. Dev.*, **22**, 1835 (2018); https://doi.org/10.1021/acs.oprd.8b00386
10. C. Jorand-Lebrun and R. Boivin, Preparation of Quinoline Compounds as IRAK Inhibitors and Uses Thereof, WO Patent 149522A1 (2019).
11. Y. Xie and L.E. Babiss, Preparation of Heterocyclic Compounds as IRAK4 Inhibitors. WO Patnet 089422A1 (2019).
12. Y. Jie, P. Livant, H. Li, M. Yang, W. Zhu, V. Cammarata, P. Almond, T. Sullens, Y. Qin and E. Bakker, *J. Org. Chem.*, **75**, 4472 (2010); https://doi.org/10.1021/jo100628v
13. I.V. Alabugin, L. Kuhn, N.V. Krivoshchapov, P. Mehaffy and M.G. Medvedev, *Chem. Soc. Rev.*, **50**, 10212 (2021); https://doi.org/10.1039/D1CS00564B
14. S.A. Glover and A.A. Rosser, *J. Org. Chem.*, **77**, 5492 (2012); https://doi.org/10.1021/jo300347k
15. K.W. Bowers, R.W. Giese, J. Grimshaw, H.O. House, N.H. Kolodny, K. Kronberger and D.K. Roe, *J. Am. Chem. Soc.*, **92**, 2783 (1970); https://doi.org/10.1021/ja00712a032
16. H.O. House, *Acc. Chem. Res.*, **9**, 59 (1976); https://doi.org/10.1021/ar50098a003
17. M. J. Frisch, G.W. Trucks, H.B. Schlegel, G.E. Scuseria, M.A. Robb, J.R. Cheeseman, G. Scalmani, V. Barone, G.A. Petersson, H. Nakatsuji, X. Li, M. Caricato, A.V. Marenich, J. Bloino, B.G. Janesko, R. Gomperts, B. Mennucci, H.P. Hratchian, J.V. Ortiz, A.F. Izmaylov, J.L. Sonnenberg, D. Williams-Young, F. Ding, F. Lipparini, F. Egidi, J. Goings, B. Peng, A. Petrone, T. Henderson, D. Ranasinghe, V.G. Zakrzewski, J. Gao, N. Rega, G. Zheng, W. Liang, M. Hada, M. Ehara, K. Toyota, R. Fukuda, J. Hasegawa, M. Ishida, T. Nakajima, Y. Honda, O. Kitao, H. Nakai, T. Vreven, K. Throssell, J.A. Montgomery, Jr., J.E. Peralta, F. Ogliaro, M.J. Bearpark, J.J. Heyd, E.N. Brothers, K.N. Kudin, V.N. Staroverov, T.A. Keith, R. Kobayashi, J. Normand, K. Raghavachari, A.P. Rendell, J.C. Burant, S.S. Iyengar, J. Tomasi, M. Cossi, J.M. Millam, M. Klene, C. Adamo, R. Cammi, J.W. Ochterski, K. Morokuma, R.L. Martin, O. Farkas, J.B. Foresman and D.J. Fox, Gaussian 16. Wallingford, CT: Gaussian, Inc. (2016).
18. R. Dennington, T.A. Keith and J.M. Millam, GaussView (Version 6.0). Shawnee, KS: Semichem Inc. (2016).